PCCP

Accepted Manuscript

ROYAL SOCIETY OF CHEMISTRY

www.rsc.org/pccp

Oxygen Vacancy and Hole Conduction in Amorphous TiO_2

Hieu H. Pham and Lin-Wang Wang

Joint Center for Artificial Photosynthesis and Materials Sciences Division

Lawrence Berkeley National Laboratory, Berkeley, California 94720

Corresponding Author: Lin-Wang Wang (lwwang@lbl.gov)

Abstract.

The amorphous titanium dioxide (a-TiO_2) has drawn attention recently due to the finding on its promise for coating conventional photoelectrodes for corrosion protection while still allowing the holes to transport to the surface. The mechanism of the hole conductivity at a level much higher than the edge of valence band is still a mystery. In this work, an amorphous TiO_2 model is obtained from molecular dynamics employing the "melt-and-quench" technique. The electronic properties, polaronic states and hole conduction mechanism in amorphous structure were investigated by means of density functional theory with Hubbard's energy correction (DFT+U) and compared to those in crystal (rutile) TiO_2. The formation energy of oxygen vacancy was found to reduce significantly (by a few eV) upon the amorphization. Our theoretical study suggested that the oxygen vacancies and their defect states provide hopping channels which are comparable with experimental observations and could be responsible for the hole conduction in the "leaky" TiO_2 recently discovered for the photochemical water-splitting applications.

Keywords. charge transfer, transition metal oxides, polarons, defect states, electronic structure, Marcus theory, DFT+U, HSE06, titanium dioxide

1. Introduction

In the last decade, titanium dioxide (TiO_2) has been one of the most studied materials due to its low cost, light weight, eco-friendliness and long-term stability to be used in photosynthesis, solar cells, electrochromic devices, rechargeable batteries, hydrogen storage and sensors [1, 2]. While the crystal TiO_2, including rutile, anatase, and brookite, have been extensively studied for their electronic structures, defect levels and polaron formations [3-7], the studies for the amorphous polymorph are relatively rare [8-11]. However, it is the amorphousness that sometimes plays crucial roles in particular applications [12, 13]. For instance, in actual technical applications, amorphous TiO_2 has been widely used, either as an active photocatalyst, substrate, or protection layer [14-20]. The electronic structures, optical properties, carrier dynamics and defect properties of such a system are obviously functions of the structural characterization. It is thus necessary to understand the role of amorphousness in TiO_2, in addition to its crystal counterparts. In this work, we perform *ab initio* calculations to study the electronic structure, native defect formation energies and polaronic states of amorphous TiO_2, and compare them to those in crystal TiO_2 (rutile TiO_2). The presence of defects can play critical role in the materials' application, while the formation energies of such defects, and their electronic structures can be very different between bulk and amorphous structures. Similarly, it has been found that the hole in some TiO_2 crystalline polymorhs could form deep localized polaron [21, 22]. Therefore, it would be interesting to investigate its counterpart in the amorphous TiO_2. In another example, it was found recently that amorphous TiO_2 could be used as a "leaky" protection layer for photo-induced water splitting [23]. While protecting the light-absorbing photoanode from corrosion, it can conduct hole carriers, perhaps through some defect levels. This discovery is an important technologically breakthrough since the adoption of such anode protection layer can enable the uses of many conventional semiconductors for water splitting applications. Nevertheless, the exact mechanism for such hole conductivity is not clearly understood. Thus a study of the defect levels in such a system might help to shed light for this particularly important issue.

The study of the amorphous TiO_2 is nontrivial because the atomic structure itself is challenging to define. Here, following the previous literature, we will use the molecular dynamics method (MD) to construct the atomic structure of a model amorphous TiO_2. This model structure yields the same atom-atom correlation function as the experimentally obtained ones while losing the long-range order of the crystal structure. The electronic structure of the

model system is then studied by means of density functional theory (DFT). This includes the hybrid functional (HSE06) [24] and the GGA+U [25] with the U parameter obtained from previous crystal TiO_2 calculations. While the possible error in using DFT to describe the electronic structure is well known, we have compared the results of crystal rutile TiO_2 (r-TiO_2) with those of amorphous TiO_2 (a-TiO_2), thus reduced the potential uncertainty by looking at their differences. Such comparison also provides us with insights why some applications are necessary for the system to be in the amorphous structure. Whenever possible, we have also applied the HSE06 calculation which is believed to be more reliable than the GGA+U, but with much higher computational cost. Through our ab initio calculations, we found that: (i) Unlike the covalent bond semiconductors, e.g., GaAsN, a "good" amorphous TiO_2 can be readily formed through MD, indicating easy kinetic process in forming such systems; (ii) The so formed amorphous TiO_2 has a clean band gap which is slightly wider than that of the rutile TiO_2. No tail density of state (DOS) is found despite of the fact that the band edge states are localized; (iii) The hole polaron can be formed with a higher polaron formation energy than that in rutile TiO_2; (iv) The O vacancy formation energy in amorphous TiO_2 can be a few eV lower than its crystal counterparts, indicates the possible prominence of such native defect; (v) Lastly, the investigation of electronic structures and the calculations of charge transfer rate by the Marcus theory suggested that the O defect state can be a potential candidate for the hole transport channels in the "leaky" amorphous TiO_2.

2. Computational Details

We used classical potential molecular dynamics (MD) method to obtain the amorphous model of titanium dioxide. The interatomic interactions between Ti-Ti, Ti-O and O-O pairs are characterized by the Matsui-Akaogi force field [26], which has shown to reproduce well the structural properties of crystalline TiO_2, as well as the liquid and amorphous forms [27]. The potential energy of this Matsui-Akaogi force field is described as a sum of pair interaction contributions representing the Coulomb, dispersion and repulsion interactions.

The amorphousness was produced using the "melt-and-quench" technique. First, the TiO_2 crystals were heated up to high temperatures (4000K, which is far above the melting point 2116 K of TiO_2 crystals) until the crystals completely lose their structural memory. This was then followed by slowly cooling to room temperature that allows the formation of the amorphous

phase. In this work, various structures (rutile, anatase, brookite) were considered as the input configurations for the production of the amorphous polymorph. The heating and cooling processes were computationally conducted with a temperature increasing/decreasing step of 200K. The time step for the MD simulations is 1 fs. At each temperature step (during the heating, as well as the cooling), the sample is equilibrated for 100 ps using the isothermal-isobaric ensemble (NPT). The obtained structures (amorphous) were then used for further atomic relaxation by means of first-principles calculations.

Density functional theory (DFT), [28] as implemented in the Vienna *ab initio* Simulation Package (VASP), [29] was employed to perform the first-principles calculations. Mostly calculations used the electron projector-augmented wave methods [30] with the PBE generalized gradient approximation (GGA) exchange–correlation [31], plus an onsite Ti d state U correction (DFT+U, or say GGA+U) [25]. A plane-wave cut-off of 400 eV was used and the magnetic moment was accounted for by performing spin-polarized energy calculations. The value of U = 4.2 was used for the on-site Coulomb correction to the Ti 3d states, which was shown to successfully describe the electronic properties and defect states in crystalline titanium dioxide [32-34]. For the k-space sampling, we used a 2x2x3 Monkhorst-Pack grid [35] for the 216-atom supercells (both r-TiO_2 and a-TiO_2) and a 4x4x4 grid for the 72-atom supercell (r-TiO_2). In case of hybrid calculations (HSE06), a single k-point (1x1x1) was used.

The formation energy of one oxygen vacancy with charge state q is calculated as follows [36, 37]:

$$\Delta H(V_O^q) = E(V_O^q) - E(clean) + \frac{1}{2}(E_O + \mu_O) + q(\epsilon_{VBM} + E_F + \Delta v) \quad (1)$$

where $E(V_O^q)$ and $E(clean)$ are the total energies of the supercell with and without the oxygen vacancy. μ_O is the elemental chemical potential of oxygen, referenced to the total energy E_O of its pure gas state (isolated O_2). Due to the well-known error in DFT calculation of O_2 binding energy [38], we therefore apply a corrected value $\Delta E_O^{corr} = 1.42\, eV/O_2$ to E_O, by taking the difference between our DFT calculated binding energy of O_2 (-6.65 eV) with the experimental one (-5.23 eV) [39]. In this work our calculations were performed in oxygen-rich conditions, i.e. μ_O = 0. E_F is the Fermi energy level referenced to the valence band maximum (VBM) eigenenergy of the initial TiO_2 system, ϵ_{VBM}. The term Δv is added for the correction of the electrostatic interaction caused by the limited size of the supercell, obtained by taking the shifting of the Ti 1s

core-level energies of a Ti atom far away from the O vacancy in the TiO_2 supercells with the neutral and charged defect states.

3. Results and Discussions

3.1. Structural characterization and effects of amorphousness on the band structure

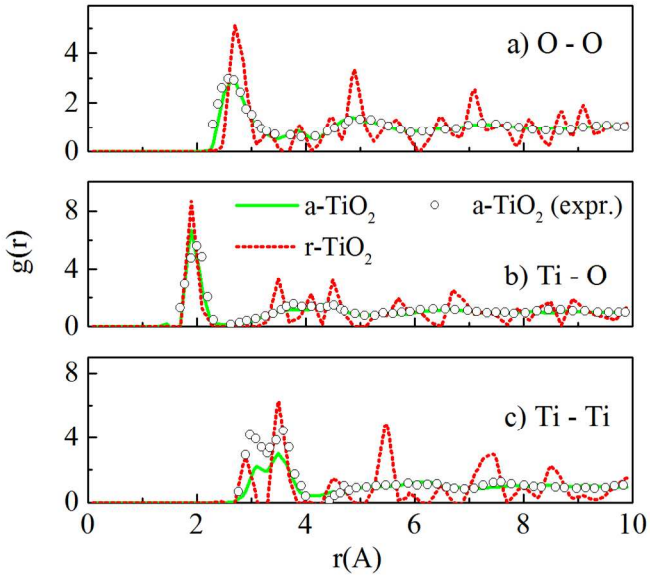

Figure 1. Radial distribution functions g(r) for a) O-O, b) Ti-O and c) Ti-Ti pairs of the amorphous (a-TiO_2) and rutile (r-TiO_2) models at 300K, using the Matsui-Akaogi force field. The experimental data for sputtered TiO_2 amorphous layers were taken from reference [15].

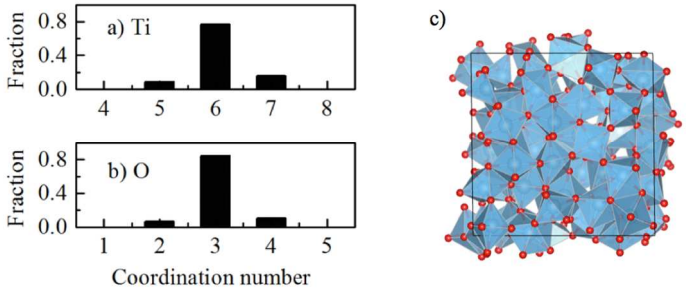

Figure 2. Coordination number distribution in amorphous TiO_2 model for a) Titanium and b) Oxygen. The cutoff distance for calculating the neighbors r = 2.6 Å. c) Final relaxed structure of the amorphous TiO_2 (obtained from "melt-and-quench" of the 216-atom rutile system), after atomic relaxation using DFT+U. Red sphere – O, blue – Ti.

The radial distribution functions (RDF) for O-O, Ti-O and Ti-Ti pairs of the amorphous structure are presented in the Figure 1. Different starting crystals were initially used for the "melt-and-quench" process, including rutile, anatase and brookite supercells (containing 216, 216 and 192 atoms, repectively). Besides, the "melt-and-quench" was also tested on an arbitrary structure of 192 atoms with Ti:O stoichiometric ratio of 1:2, in which the initial atomic positions are randomly distributed. It showed that final amorphous structures, obtained from different initial TiO_2 configurations, have identical structural characteristics. This confirmed that the melting process has completely eliminated the structural memory and the amorphous model is independent of its input structures. The RDF and peaks shown in Figure 1 are quite comparable with the experimental measurements on sputtered TiO_2 amorphous layers [15]. In addition, our calculations also match the results reported previously by Hoang et al. using the same potential [27].

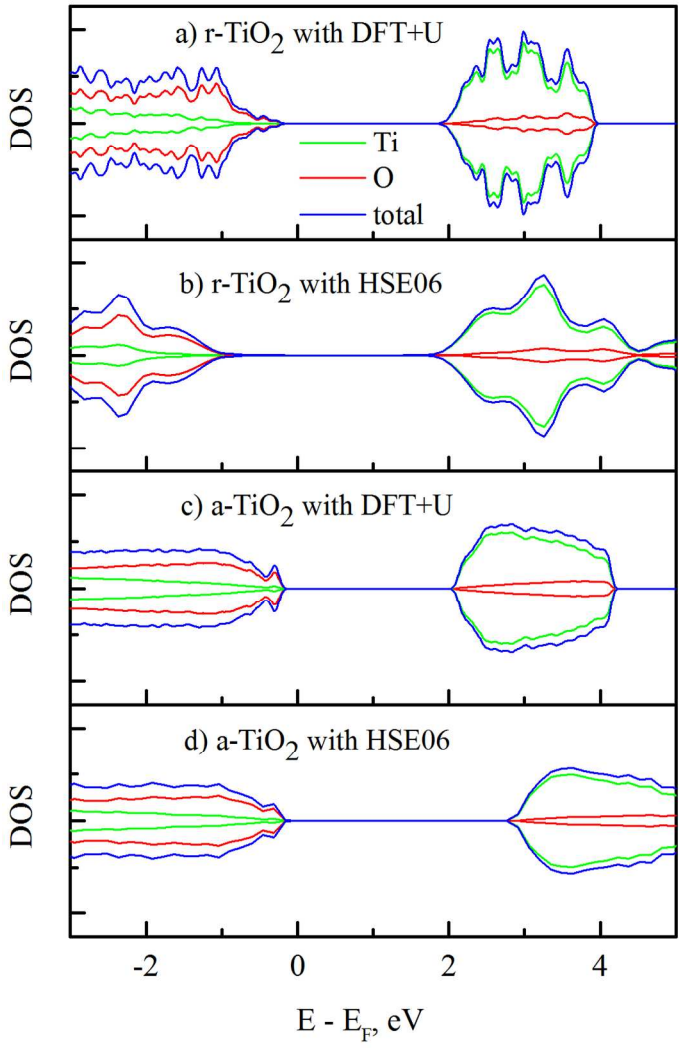

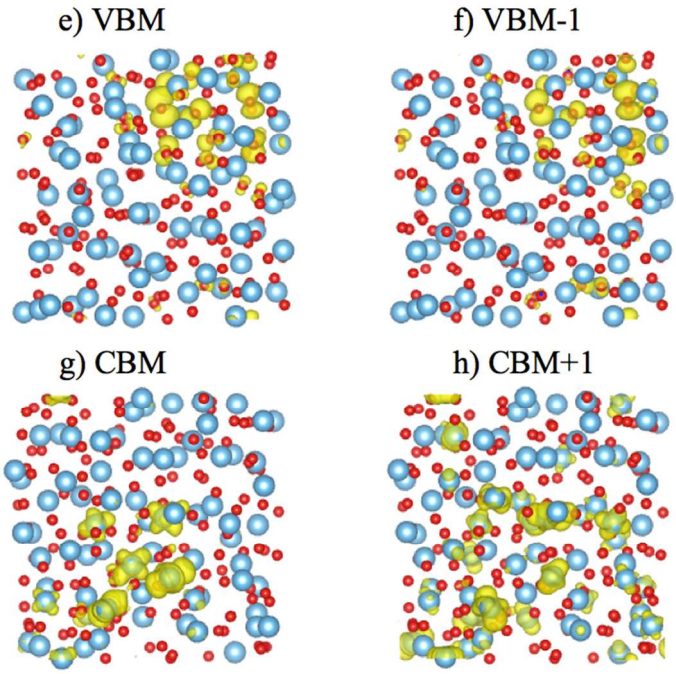

Figure 3. (a-d) Density of states of rutile and amorphous TiO_2 calculated using DFT+U and HSE06. (e-h) Band decomposed wave function isosurfaces of the band edge states in amorphous TiO_2 (results displayed for DFT+U).

It was seen that the amorphous TiO_2 model consists of staggered chains of Ti-centered octahedra sharing either the edge or the corner (Figure 2c), i.e. the local Ti-O bonding is preserved. In other words, most of Ti is surrounded by six O atoms and each O commonly has three Ti neighbors. However, there is a certain amount of Ti with 5-fold or 7-fold coordination; and similarly, O with "non-perfect" coordination number (2-fold or 4-fold coordinated), as seen in the Figure 2. This observation was also previously reported from both computational and experimental measurements [13, 15, 27, 40]. In addition, further charge analysis by the Bader method [41, 42] based on DFT+U calculations revealed that the strong charge transfer between Ti cations and O anions is preserved, and this could be the driving force for preservation of the nearest neighbor Ti-O bonding in the amorphous phase.

The calculations on electronic properties of amorphous TiO_2 to this end will be performed on the sample obtained from "melt-and-quench" of a rutile supercell (216 atoms), and for the comparison purpose we used two rutile supercells (with 72 and 216 atoms) to study the electronic properties of TiO_2 crystal. Interestingly, the amorphous TiO_2 has a clean band gap

(Figure **3**), despite the noticeable structural disorder and non-perfect coordination numbers. This is in contrast with the situation in covalent bonded semiconductors, e.g. GaAsN, where a good amorphous structure is difficult to obtain from molecular dynamics simulation, and non-perfect coordination often lead to band gap states [12]. This is also consistent with the conclusion from recent theoretical studies that amorphization introduces deep defect states or carrier-recombination centers in covalent systems but not in ionic materials [43]. Similar to crystalline TiO_2, the conduction band edge in amorphous structure is derived from Ti 3d orbitals and the valence band maximum consists mostly of the O 2p orbitals. To correct the well-known band gap underestimation by GGA, we performed additional calculations with the non-local hybrid functional (HSE06) [24], using the pre-optimized structure from the DFT+U method. The band gap of amorphous TiO_2 obtained by the HSE06 method is 3.2 eV, that agrees with experimental data reported for its optical gap between 3.2 – 3.4 eV [44-47]. The hybrid calculation for rutile band gap (2.91 eV) is also close to that from experimental measurements (3.06 eV) [48]. Figure 3, nevertheless, indicates that the charge delocalization of the band edges is strongly affected by the long-range structural disorder. Both the top of the valence band and the bottom of the conduction band are confined to certain regions in the supercell, instead of being delocalized all over the cell. This is consistent with theoretical observations previously reported for amorphous TiO_2 and GaN [10, 11, 17, 49]. Also, it is believed that the characterization of the band edges would play an essential role in establishing the polaronic or band-like natures of charge carriers [50].

3.2. Trapping of holes and the polaronic states in the amorphous TiO_2

The hole in the defect-free system is simulated by removing one electron from the valence band maximum, while the charge neutrality is maintained by a compensating uniform charge background. Despite the localization of VBM as seen in Figure 3, this free hole, without the structural re-optimization, still spreads out over a major part of the supercell and no mid-gap state was induced (Figure 4a). When the structural relaxation is allowed, we found that the hole polaron could be formed quite naturally (without the help of initial lattice displacement) and this gives rise to a clear mid-gap state of approximately 0.6 eV above the valence band (Figure 4c). Generally in crystal, the localization of charge carrier in crystals requires an initial structural perturbation in order to break the symmetry and trigger the polaronic trapping; otherwise the lattice relaxation will end up in a local minimum with the free (delocalized) charge carrier [51-53].

In crystalline TiO_2 such as rutile and anatase, it is expected that the deep trapping of the charge carriers, if formed, is usually located on single Ti or O, subsequently form small polarons [3, 22, 32]. The self-trapped hole in the amorphous phase, as seen in Figure 4c however, could be localized on several O anions, instead of a single O. In other words, there could be a tendency for large hole polarons to form in the amorphous phase. This of course is aided by the original localization of the VBM state in the amorphous phase before atomic relaxation. In a way, the exact definition of the polaron state is a bit blur here due to the lack of true extended state even before atomic relaxation. The existence of this "molecular polaron" (weak polaron) has been reported by either theoretical investigations or experimental measurements in several oxides, including anatase TiO_2, doped $BaTiO_3$, $KNbO_3$ and SiO_2 [54-57].

The self-trap energy E_{ST} of the polaronic hole is defined as the difference between the initial atomic structure energy (with the free/delocalized hole) and the energy of atomic relaxed system with the localized hole. Using the same U parameter in the DFT+U calculations ($U[Ti_d]$=4.2), the self-trap energies for the hole in the amorphous and rutile TiO_2 were calculated as -1.3 and +0.5 eV, respectively. The positive value obtained for rutile, within this framework, suggests that the localization of the hole could be one of local minima instead of the global one. With the help of structural distortion to break the symmetry, the free (delocalized) charge can be forced to partially localize at some O atom and this induces a tail state on the valence band (Figure 4d). In a separate calculation, further incorporation of $U[O_p]$=5.25 [3] yields a stronger localization of hole for the rutile crystal but the self-trap energy is still slightly positive (+85 meV). However, some theoretical works have shown the formation of hole polaron both at the surface and in the doped bulk rutile TiO_2 [58-61]. But it was also proposed that acceptor states could be deep in anatase but are shallow in rutile [21, 62]; in addition, the self-trapped and delocalized hole states could be energetically comparable [59, 63]. Our DFT+U results here are supportive of the shallow rutile polaron hypothesis.

Our calculations therefore have suggested the trend that the self-trap energy of hole in amorphous structure is much larger than its rutile counterpart. There could be several reasons for this observation. Firstly, the VBM of a-TiO_2 before atomic relaxation is somehow already localized. Thus, further localization will not cause much kinetic energy due to wave function confinement [53]. Secondly, the chemical bonds near the VBM state might not be as strong as those in the crystal structure. The relative imperfect and hence loose chemical bonds result in more

pronounced atomic relaxations, therefore deepens the trapping energy. The effective volume of wave function ($V_{hole} = 1/\int|\psi_{hole}(r)|^4\, d^3r$) for the hole states before and after the atomic relaxations are 66.2 and 5.6 Å^3, respectively. This indicated a significant localization of charge as a result of structural optimization. The hole wave functions are also shown as insets in Figure 4.

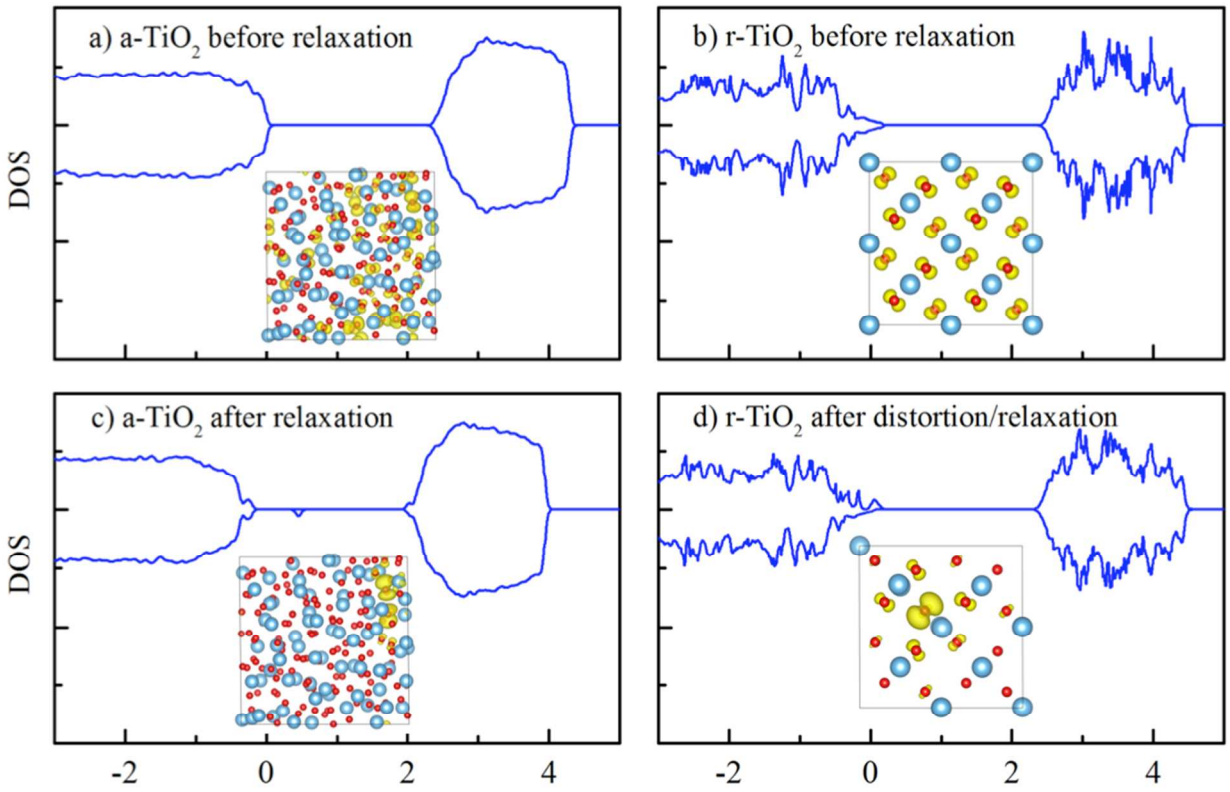

Figure 4. a) Density of states for amorphous and rutile TiO_2 with a hole in the supercell (one electron is removed from the volume of the supercell): a) a-TiO_2 before the lattice relaxation, b) r-TiO_2 before the lattice relaxation, c) a-TiO_2 after the lattice relaxation, and d) r-TiO_2 after the lattice distortion and subsequent optimiztion. The insets show the charge density isosurfaces of the hole states in correspoding systems. Blue sphere denotes Ti and red sphere - O.

3.3. Oxygen vacancy defect states in amorphous TiO_2

We have calculated the oxygen vacancy formation energy V_O^0 in different TiO_2 phases (in the oxygen-rich condition) and the comparison is presented in the Table 1. It was shown that the formation of V_O^0 in the amorphous structure is energetically much more favorable. Surprisingly,

the formation energy in a-TiO_2 could be lower by as much as 3 or 4 eV, compared to that in crystalline TiO_2. This is probably due to the intrinsic bonding frustration in the amorphous structure [64]. However, the $\Delta H(V_O^0)$ value could be different from site to site. We observed that the oxygen atoms, at which the VBM state is localized (as shown in Figure 3d), are the most favorable sites for the vacancy formation (which are the values presented in Table 1). Consider however that our supercell consists of only 216 atoms (144 oxygen sites), such favorable sites are rather abundant. Our calculations also indicated that the formation of the bi-vacancy (two vacancies at nearest neighboring sites) could be energetically favorable, compared to two separate vacancies, in TiO_2 crystal (rutile). However, it is not necessarily the case in a-TiO_2, where we found a positive binding energy of vacancies to form the bi-vacancy.

The calculated O vacancy formation energies $\Delta H(V_O^q)$ for different charge state q in the amorphous and rutile supercells are plotted in the Figure 5 as a function of Fermi energy (shifting from the valence band maximum, E_F = 0). It indicated that the oxygen vacancy could exist in three charge states (neutral, +1 and +2) in amorphous TiO_2, as well as in rutile. At Fermi levels near the VBM, the positively charged V_O^{+1} and V_O^{+2} could form spontaneously in amorphous TiO_2. When the Fermi energy increases, the formation energy of the positively charged defect increases, until the transaction to the neutral state occurs. The transitions from V_O^0 to V_O^{+1} (denoted as $\epsilon^{0/+1}$) and from V_O^{+1} to V_O^{+2} ($\epsilon^{+1/+2}$) were all observed within the band gap (Figure **5**) for both phases (amorphous and rutile). In the amorphous structure, these turning points (both $\epsilon^{0/+1}$ and $\epsilon^{+1/+2}$) are deeper below the CBM, compared to those in the rutile.

Table 1. Formation energy of the neutral-charged oxygen vacancy $\boldsymbol{V_O^0}$ in different phase of TiO_2 at oxygen-rich conditions, using DFT+U method

	rutile	anatase	brookite	amorphous
$\Delta H(V_O^0)$, eV	5.59	4.42	5.20	1.35

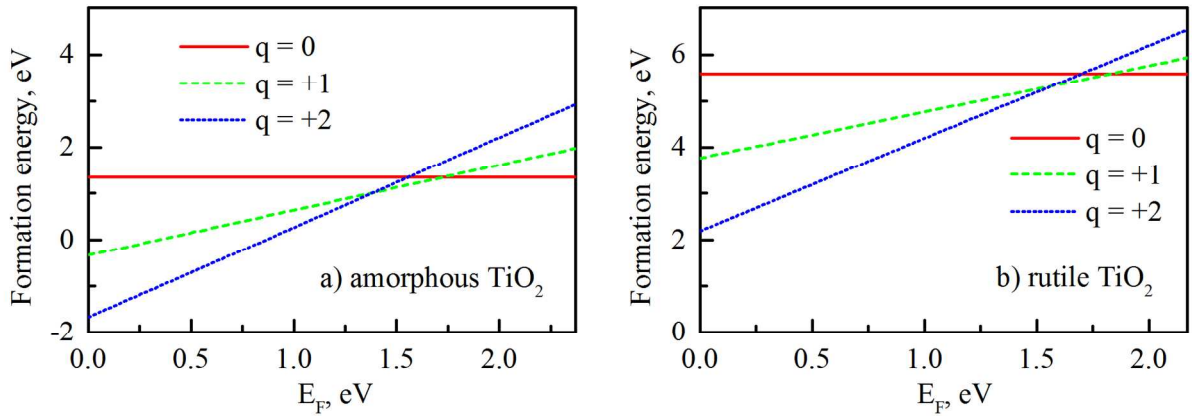

Figure 5. Formation energy of oxygen vacancy at different charge states in: a) amorphous and b) rutile titanium dioxide (DFT+U calculations). The oxygen-rich conditions were used in the equation (1)

Herein we present further analysis on the mid-gap states induced by vacancies V_O^0, V_O^{+1} and V_O^{+2} in Figure 6. The removal of one neutral oxygen results in two unbound electrons and it was commonly accepted that these excess electrons are localized on surrounding Ti sites and subsequently form Ti^{3+} in rutile and anatase, i.e. the (neutral) oxygen vacancy comes in complex with two Ti^{3+} sites [64, 65]. The corresponding Ti^{3+} peaks have been observed at 1.2 eV and 0.75 eV below the CBM in rutile [5]. Similarly, deep traps 0.9 eV and 0.5 eV below the conduction band edge, identified with transient spectroscopy, were also reported in anatase [66]. According to our DFT+U calculations, the mid-gap states in reduced amorphous TiO_2 are located at 1.9 and 1.6 eV below the conduction band minimum (Figure 6b). The locations of these impurity states within the band gap were further confirmed by performing additional HSE06 calculations (for the correction of the band gap) and it showed that the peaks are at 1.7 and 1.6 eV below the CBM, consistent with the DFT+U results. Thus, our calculated amorphous TiO_2 neutral O vacancy levels are deeper from the conduction band than the experimentally measured levels in rutile and anatase. However, this is consistent with the fact that our calculated V_O^0/V_O^{+1} transition level in amorphous TiO_2 is lower than that of rutile as shown in Figure 5 counting from the conduction band.

If one occupied impurity electron is removed from the system, i.e. the vacancy now becomes V_O^{+1}, the impurity states are separated into two states (one occupied and one empty) with a significant energy gap, as displayed in Figure 6(c-d). The unoccupied level is initially

located near the conduction band edge if the V_O^0 state atomic position is used. After atomic relaxation, the empty state moves up in energy and subsequently merges into the conduction band. Meanwhile, the other occupied state stays at 1.9 eV below the CBM. When both of electrons are removed together with the oxygen (V_O^{+2}), these unoccupied states could be seen in the band gap before the relaxation (Figure 6e). After the structural relaxation, these (empty) energy states are shifted up and merge with the conduction band and therefore return a clear band gap again. This finding is consistent with other oxides or ionic systems: when an ion is removed with its normal valence state (e.g., O^{2-}), no gap state will exist after the structural relaxation [67].

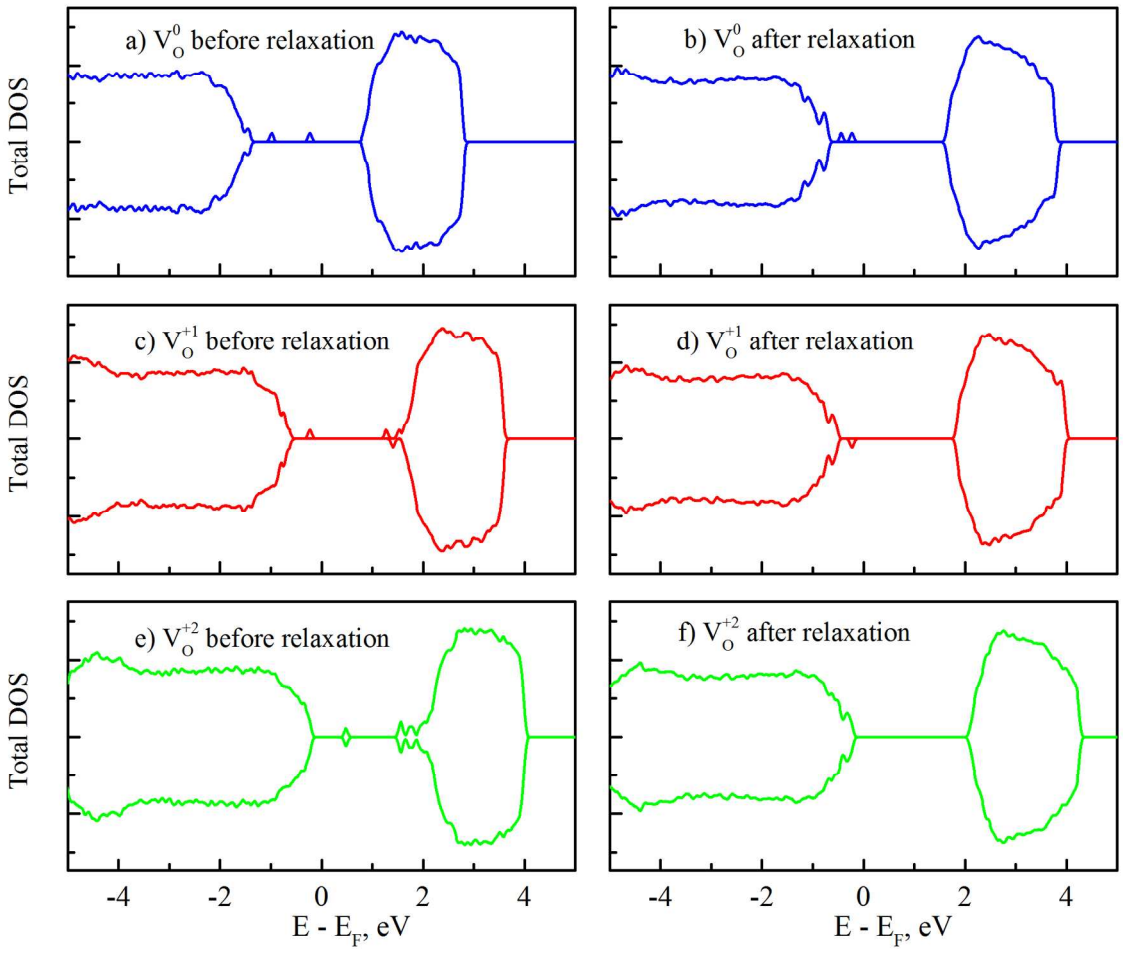

Figure 6. Density of states (from DFT+U calculations) of the amorphous TiO_2 with the oxygen vacancy in different charge states (before and after structural relaxation): a-b) neutral vacancy, c-d) vacancy with charge +1 and e-f) vacancy with charge +2

3.4 The defect induced hole conductivity in amorphous TiO_2

After the investigations of structure, polaron and defect states in amorphous TiO_2, we now like to discuss the possible mechanisms of hole conduction in the "leaky" amorphous TiO_2 protection layer as reported in the recent discovery by Hu et al. [23]. In fact, the mechanism of the hole conductivity reported in Ref. [23] was not clear. It was suspected that N and C impurities, or other defects related to amorphous TiO_2 might play a role. One interesting phenomenon is the existence of a weak density of state peak in the X-ray induced electron emission spectrum [23]. This peak is at approximately 1.5 eV above the top of valence band and in the order of 1% compared to the main peak. The reported secondary-ion mass spectrometry data counts for N and C indicate that they might be four orders of magnitudes smaller than that of Ti, thus perhaps too dilute to account for the 1% electronic density of state. Furthermore, it was reported that [23], the hole conduction was no longer observed after thermo annealing (also disappeared is the 1% defect density of state), while the N and C contents remain (although the crystallinity/amorphousness of the system might also have changed). All these prompt us to propose that the O vacancy in amorphous TiO_2 could be one hole conduction channel. Due to the relative small formation energy as shown in Table 1 and Figure 5a, and the kinetic process in sputtering such thin film, the neutral O vacancy can be formed, perhaps with a concentration around 1%. Many of the oxides can have such small off-stoichiometry, especially the oxygen deficit. Since the TiO_2 amorphous thin film is n-type, the O vacancy should be in neutral state. Our calculation shows that (Figure 6b) such O vacancy can produce occupied impurity density of states above the VBM. Note that, our calculated impurity states shown in Figure 6b is too close to the VBM compared to the X-ray photoelectron emission measured impurity density of state (which is about 1.5 eV above the VBM [23]). However, when we compared with such X-ray induced electron emission spectrum, we should really compare the average of the density of states of V_O^0 and V_O^{1+} (before and after the electron has been emitted, and both at the V_O^0 atomic structure); in other words, taking the average of the higher peaks in Figure 6b and Figure 6c. As a result, the averaged peak should be around 1.5 eV above VBM, hence in good agreement with the experimental data (one can also take the total energy difference before and after removing one electron from the impurity state with the V_O^0 atomic structure, such result is usually very close to the above averaging procedure). As for the disappearance of impurity state and the hole conductivity after thermal annealing, one natural interpretation is the filling of such O vacancy

during the thermal annealing. In addition, one might also consider the direct polaron transport without the O vacancy; however, the polaron level might be too close to the VBM level. Besides, there is no defect impurity state within the gap without O vacancy, therefore inconsistent with the X-ray photoelectron emission data.

In order to evaluate the extent of hole conductivity resulted from the O vacancies, we use the Marcus theory to study the hole hopping rate from one O vacancy to a neighboring one. Since we assume the vacancy concentration at about 1% (which is approximately the same amount as in our defect amorphous supercell), we can use the hopping from one O vacancy to its periodic image to estimate this transfer rate. The charge transfer rate $1/\tau$, according to the Marcus theory, could be calculated as follows [68, 69]:

$$\tau^{-1} = V_c^2 \sqrt{\frac{\pi}{\lambda k_B T \hbar^2}} \exp\left[-\frac{(\lambda + E_f - E_i)^2}{4\lambda k_B T}\right] \quad (2)$$

where k_B is the Boltzmann constant, $\hbar$ is the Planck constant, T is temperature, λ is the reorganization energy of the system when the hole is transferred from one site to another, and V_c is the electronic coupling between two states involved in the transfer. In our work, this state-state coupling V_c was estimated from the impurity state k-point dispersion in a periodic box. According to a simple one band tight-binding model, the band energy difference between the supercell Γ and X points is $4V_c$. The E_i and E_f represent the total energy of the system before and after the hole transfer between neighboring defect sites (in this specific case, we use $E_f = E_i$). Using a random walk formula in a square lattice, the carrier mobility μ can be given by [54]:

$$\mu = 6eb^2/(\tau k_B T) \quad (3)$$

here e is the elementary charge and b is the supercell lattice (which corresponds to the hopping distance in our calculation).

Table 2. Hole transfer parameters and mobility via O-defect channel in amorphous TiO_2 (room temperature). The DFT* and HSE06* calculations were performed using the pre-optimized structures by DFT+U (see main text for details).

Calculation method	λ, eV	V_c, meV	τ, ns	μ, $cm^2 V^{-1}s^{-1}$
DFT+U	1.14	1.5	1856	2.5×10^{-6}

DFT	0.23	2.6	0.04	1.1×10^{-1}
DFT*	0.24	2.4	0.05	0.9×10^{-1}
HSE06*	0.79	2.3	23	2.0×10^{-4}

The calculated values of τ and μ for hole transfer via the O-defect channel in amorphous TiO_2 at room temperature are tabulated in Table 2. According to Marcus theory, the transition rate depends sensitively on the reorganization energy λ. Here the λ due to the hole charge transfer is calculated as: $E_{N-1}(R(V_O^0)) - E_{N-1}(R(V_O^{1+})) + E_N(R(V_O^{1+})) - E_N(R(V_O^0))$, where E_{N-1} and E_N are energies for N-1 electron and N electron (neutral) systems. $R(V_O^0)$ and $R(V_O^{1+})$ indicate the energies that are calculated at the relaxed atomic structures of the neutral and 1+ charged O vacancies, respectively. Our calculated λ and the resulting μ from the DFT+U (U=4.2 eV) and the DFT (GGA) results are very different. The DFT+U λ is 0.9 eV larger than the DFT result. This is because the DFT+U has a tendency to overestimate the wave function localization, while plain DFT tends to make the wave function delocalized. In this regard, the HSE06 should be a function that is more reliable. Therefore, we have also performed HSE06 calculations. However, it is quite computationally expensive to obtain the relaxed atomic structures using HSE06 for several-hundred-atom systems, thus we have estimated this λ using formula: $E_{N-1}(R'(V_O^0)) - E_{N-1}(R'(V_O^{1+})) + E_N(R'(V_O^{1+})) - E_N(R'(V_O^0))$, and called the result λ* as indicated in Table 2. Here the R' are the relaxed atomic positions taken from DFT+U calculations, while the energy E_{N-1} and E_N are evaluated using self-consistent HSE06 calculations. To test the accuracy of this procedure, we have used the same formula to calculate DFT λ, and the resulting DFT λ* and hole mobility are very similar to the original DFT values (Table 2). As a matter of fact, this can be a rather general procedure to evaluate the reorganization energy of a charge transfer process under an expensive functional using the atomic positions of another inexpensive calculation. To illustrate why this procedure is reliable, we offer the following explanation.

A schematic diagram for how to calculate the relaxation energy λ in a charge transfer problem is displayed in Figure 7. Note that, this diagram is slightly different from the conventional Marcus diagram, since when the hole hops from the E_{N-1} system to the E_N one, both systems will relax and contribute to the reorganization energy. Assuming both E_{N-1} and E_N have

a quadratic form of $\frac{1}{2}\kappa(R-R_0)^2$ at their corresponding minimum points R_0, then the reorganization energy can be calculated as (Figure 7a):

$$\lambda = E_{N-1}(B) - E_{N-1}(C) + E_N(D) - E_N(A) = \kappa\Delta R^2 \quad (4)$$

where ΔR is the position shift $R(V_O^0) - R(V_O^{1+})$ or say between B and C (D and A) points. Now, if DFT+U atomic configurations are used (instead of the HSE06 ones), the A, B, C, D points are shifted to A', B', C', D' points as illustrated in Figure 7b. However, under the zeroth order approximation, it could be a good approximation that the A', B', C', D' are disturbed from their corresponding A, B, C, D positions by a common shift δ. As a result, we have:

$$\begin{aligned}\lambda^* &= E_{N-1}(B') - E_{N-1}(C') + E_N(D') - E_N(A') \\ &= \tfrac{1}{2}\kappa[(\Delta R+\delta)^2 - \delta^2] + \tfrac{1}{2}\kappa[(\Delta R-\delta)^2 - \delta^2] = \kappa\Delta R^2 \end{aligned} \quad (5)$$

Thus λ and λ* come out to be identical.

Our calculated λ* by the above HSE06* approach is 0.79 eV and the state-state coupling V_c is about 2.3 meV. As a result, the hole hopping time τ is 23 ns. This τ yields a mobility of 2.0×10^{-4} $cm^2\ V^{-1}s^{-1}$ at room temperature. Unfortunately, experimental data on the mobility and hole transfer even in crystal TiO_2 are quite limited [70]. The hole mobility of undoped rutile TiO_2 measured by Odier et al. based on the Hall effect method is 0.1 ($cm^2\ V^{-1}s^{-1}$) at 1300K [71]. Recently, Deskins et al. [54] have calculate the hole polaron mobility in rutile TiO_2 as 0.16 ($cm^2\ V^{-1}s^{-1}$) at 1300K, and 5.1×10^{-3} at 298K. Thus, our amorphous TiO_2 mobility via the O vacancy channel is approximately only one order of magnitude smaller than the corresponding bulk crystal mobility. We believe that might be mobile enough to provide the hole leaky channel in the amorphous TiO_2 protection layer. We also note that, there is a possibility to lower the total energy (raise the hole level) a little bit after each charge transfer ($E_f - E_i < 0$ in Eq. 2). That can significantly enhance the transition rate at the expense of losing some potential after the charge transport.

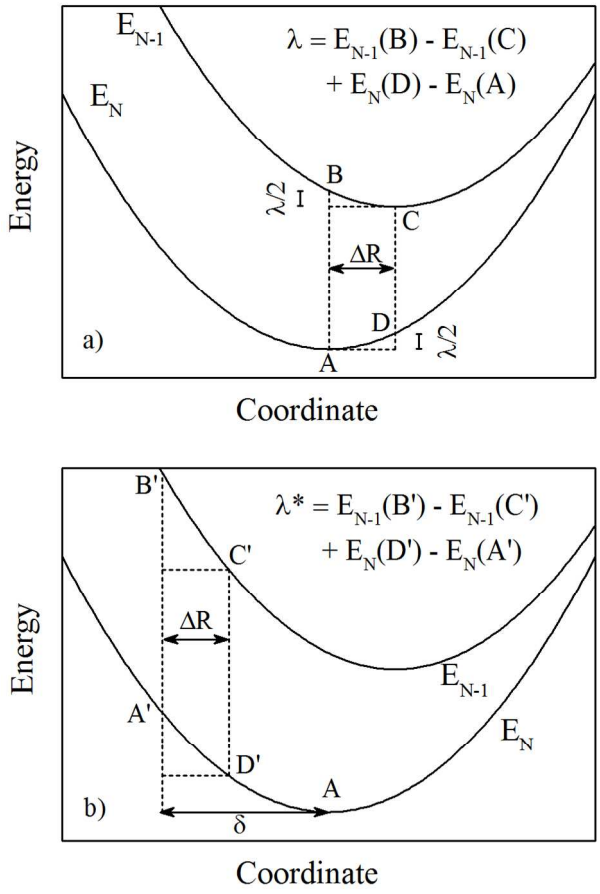

Figure 7. Schematic diagram for calculations of hole-transfer reorganization energy λ. The E_{N-1} and E_N correspond to states with and without a hole (neutral charge), respectively. a) Both final configurations before and after charge transfer are the ground states. ΔR is the structural relaxation due to the presence of one hole. This scheme corresponds to cases of fully relaxed structures for a given energy functional, as used in regular DFT and DFT+U calculations. b) All configurations before and after charge transfer are shifted from the ground states by a value δ. This scheme corresponds to cases of DFT* and HSE06* in Table 2, in which the pre-optimized structures from DFT+U are used for the energy calculations.

4. Conclusions

In summary, we have investigated the possible mechanism of hole conduction in amorphous TiO_2 via defect states. We have proposed that the amorphization and the favorable formation of oxygen vacancy in a-TiO_2 could promote the hole transport. Specifically, the O defect state could serve as a hole transfer channel at about 1-1.5 eV above the VBM and be

responsible for the good conductivity in the recently discovered "leaky" ALD-TiO_2 coating layer for water-splitting photoanodes [23].

In the amorphous TiO_2 structure, the nearest neighbor Ti-O bonding and local octahedral configurations are preserved. The long-range disorder and imperfect coordination of Ti and O do not induce defect states in the band gap but have effects on the localization of band edge states. The trapping of holes can occur naturally without initial lattice distortion. The structural disorder upon amorphization results in a substantial reduction of O vacancy formation energy; as a result, the O vacancy in amorphous TiO_2 could be much more abundant than its crystal counterparts. The neutral O vacancy is a deep donor in amorphous TiO_2. The calculated O vacancy photoemission peak should be in the range of 1-1.5 eV above the edge of valence band, in good agreement with the experimentally measured X-ray emission data for the impurity states [23]. At around 1% O vacancy concentration, the estimated hole mobility via the O vacancy channel is about 10 times lower than the hole polaron mobility in bulk rutile TiO_2. Thus, we believe the O vacancy is capable of providing a "leaky" channel in the middle of the band gap for the a-TiO_2 protection layer reported in Hu et al. [23]

Notes

The authors declare no competing financial interests.

ACKNOWLEDGMENTS

We would like to thank Dr. S. Hu for very helpful discussions. This material is based on the work performed by the Joint Center for Artificial Photosynthesis, a DOE Energy Innovation Hub, supported through the Office of Science of the U.S. Department of Energy under Award number DE-SC0004993. We use the resource of National Energy Research Scientific Computing center (NERSC) located in Lawrence Berkeley National Laboratory.

REFERENCES

1. A. Fujishima and K. Honda, *Nature*, 1972, 238, 37-+.
2. X. Chen and S. S. Mao, *Chem Rev*, 2007, 107, 2891-2959.
3. B. J. Morgan and G. W. Watson, *Phys Rev B*, 2009, 80.
4. M. Landmann, E. Rauls and W. G. Schmidt, *J Phys-Condens Mat*, 2012, 24.
5. D. C. Cronemeyer, *Phys Rev*, 1959, 113, 1222-1226.
6. C. Di Valentin, G. Pacchioni and A. Selloni, *Phys Rev B*, 2004, 70.
7. B. J. Morgan, D. O. Scanlon and G. W. Watson, *J Mater Chem*, 2009, 19, 5175-5178.
8. S. K. Deb, *Solid State Commun*, 1972, 11, 713-&.
9. V. A. Bakaev and W. A. Steele, *Langmuir*, 1992, 8, 1372-1378.
10. M. Landmann, T. Kohler, S. Koppen, E. Rauls, T. Frauenheim and W. G. Schmidt, *Phys Rev B*, 2012, 86.
11. B. Prasai, B. Cai, M. K. Underwood, J. P. Lewis and D. A. Drabold, *J Mater Sci*, 2012, 47, 7515-7521.
12. E. B. Kandemir, B. Gonul, G. T. Barkema, K. M. Yu, W. Walukiewicz and L. W. Wang, *Comp Mater Sci*, 2014, 82, 100-106.
13. H. Z. Zhang, B. Chen, J. F. Banfield and G. A. Waychunas, *Phys Rev B*, 2008, 78.
14. M. Kanna and S. Wongnawa, *Mater Chem Phys*, 2008, 110, 166-175.
15. V. Petkov, G. Holzhuter, U. Troge, T. Gerber and B. Himmel, *J Non-Cryst Solids*, 1998, 231, 17-30.
16. R. D. Eithiraj and K. R. Geethalakshmi, *Chem Phys Lett*, 2013, 585, 138-142.
17. K. K. Ghuman and C. V. Singh, *J Phys-Condens Mat*, 2013, 25.
18. T. Kohler, M. Turowski, H. Ehlers, M. Landmann, D. Ristau and T. Frauenheim, *J Phys D Appl Phys*, 2013, 46.
19. Z. Y. Zhang and P. A. Maggard, *J Photoch Photobio A*, 2007, 186, 8-13.
20. S. D. Standridge, G. C. Schatz and J. T. Hupp, *Langmuir*, 2009, 25, 2596-2600.
21. P. Deak, B. Aradi and T. Frauenheim, *Phys Rev B*, 2011, 83.
22. S. Y. Chen and L. W. Wang, *Phys Rev B*, 2014, 89.
23. S. Hu, M. R. Shaner, J. A. Beardslee, M. Lichterman, B. S. Brunschwig and N. S. Lewis, *Science*, 2014, 344, 1005-1009.
24. J. Paier, M. Marsman, K. Hummer, G. Kresse, I. C. Gerber and J. G. Angyan, *J Chem Phys*, 2006, 125.
25. S. L. Dudarev, G. A. Botton, S. Y. Savrasov, C. J. Humphreys and A. P. Sutton, *Phys Rev B*, 1998, 57, 1505-1509.
26. M. Matsui and M. Akaogi, *Mol Simulat*, 1991, 6, 239-244.
27. V. V. Hoang, *Phys Status Solidi B*, 2007, 244, 1280-1287.
28. W. Kohn and L. J. Sham, *Phys Rev*, 1965, 140, 1133-&.
29. G. Kresse and J. Furthmuller, *Phys Rev B*, 1996, 54, 11169-11186.
30. P. E. Blochl, *Phys Rev B*, 1994, 50, 17953-17979.
31. J. P. Perdew, K. Burke and M. Ernzerhof, *Phys Rev Lett*, 1996, 77, 3865-3868.
32. B. J. Morgan and G. W. Watson, *Phys Rev B*, 2010, 82.
33. B. J. Morgan and G. W. Watson, *J Phys Chem C*, 2009, 113, 7322-7328.
34. P. M. Kowalski, M. F. Camellone, N. N. Nair, B. Meyer and D. Marx, *Phys Rev Lett*, 2010, 105.
35. H. J. Monkhorst and J. D. Pack, *Phys Rev B*, 1976, 13, 5188-5192.
36. S. Lany and A. Zunger, *Phys Rev B*, 2009, 80.

37. S. Y. Chen and L. W. Wang, *Appl Phys Lett*, 2011, 99.
38. K. A. Persson, B. Waldwick, P. Lazic and G. Ceder, *Phys Rev B*, 2012, 85.
39. J. A. Pople, M. Headgordon, D. J. Fox, K. Raghavachari and L. A. Curtiss, *J Chem Phys*, 1989, 90, 5622-5629.
40. K. Kaur, S. Prakash, N. Goyal, R. Singh and P. Entel, *J Non-Cryst Solids*, 2011, 357, 3399-3404.
41. R. Bader, *Atoms in Molecules: A Quantum Threory*, Oxford University Press, New York, 1990.
42. G. Henkelman, A. Arnaldsson and H. Jonsson, *Comp Mater Sci*, 2006, 36, 354-360.
43. H. X. Deng, S. H. Wei, S. S. Li, J. B. Li and A. Walsh, *Phys Rev B*, 2013, 87.
44. S. B. Amor, L. Guedri, G. Baud, M. Jacquet and M. Ghedira, *Mater Chem Phys*, 2003, 77, 903-911.
45. H. Takikawa, T. Matsui, T. Sakakibara, A. Bendavid and P. J. Martin, *Thin Solid Films*, 1999, 348, 145-151.
46. Z. W. Zhao, B. K. Tay, S. P. Lau and G. Q. Yu, *J Cryst Growth*, 2004, 268, 543-546.
47. M. Zhang, G. Q. Lin, C. Dong and L. S. Wen, *Surf Coat Tech*, 2007, 201, 7252-7258.
48. A. Welte, C. Waldauf, C. Brabec and P. J. Wellmann, *Thin Solid Films*, 2008, 516, 7256-7259.
49. B. Cai and D. A. Drabold, *Phys Rev B*, 2011, 84.
50. M. D. Johannes, K. Hoang, J. L. Allen and K. Gaskell, *Phys Rev B*, 2012, 85.
51. J. B. Varley, A. Janotti, C. Franchini and C. G. Van de Walle, *Phys Rev B*, 2012, 85.
52. S. P. Ong, Y. F. Mo and G. Ceder, *Phys Rev B*, 2012, 85.
53. A. Janotti, C. Franchini, J. B. Varley, G. Kresse and C. G. Van de Walle, *Phys Status Solidi-R*, 2013, 7, 199-203.
54. N. A. Deskins and M. Dupuis, *J Phys Chem C*, 2009, 113, 346-358.
55. T. Varnhorst, O. F. Schirmer, H. Krose, R. Scharfschwerdt and T. W. Kool, *Phys Rev B*, 1996, 53, 116-125.
56. E. A. Kotomin, R. I. Eglitis, A. V. Postnikov, G. Borstel and N. E. Christensen, *Phys Rev B*, 1999, 60, 1-5.
57. S. Sicolo, G. Palma, C. Di Valentin and G. Pacchioni, *Phys Rev B*, 2007, 76.
58. A. Iwaszuk and M. Nolan, *J Phys-Condens Mat*, 2011, 23.
59. P. Zawadzki, A. B. Laursen, K. W. Jacobsen, S. Dahl and J. Rossmeisl, *Energ Environ Sci*, 2012, 5, 9866-9869.
60. Y. F. Ji, B. Wang and Y. Luo, *J Phys Chem C*, 2014, 118, 1027-1034.
61. A. Stashans and S. Bermeo, *Chem Phys*, 2009, 363, 100-103.
62. T. Yamamoto and T. Ohno, *Phys Chem Chem Phys*, 2012, 14, 589-598.
63. P. Zawadzki, K. W. Jacobsen and J. Rossmeisl, *Chem Phys Lett*, 2011, 506, 42-45.
64. A. Janotti, J. B. Varley, P. Rinke, N. Umezawa, G. Kresse and C. G. Van de Walle, *Phys Rev B*, 2010, 81.
65. A. Malashevich, M. Jain and S. G. Louie, *Phys Rev B*, 2014, 89.
66. T. Miyagi, M. Kamei, T. Mitsuhashi and A. Yamazaki, *Appl Phys Lett*, 2003, 83, 1782-1784.
67. D. Zherebetskyy and L.-W. Wang, *Advanced Materials Interfaces*, 2014, DOI: 10.1002/admi.201300131.
68. R. A. Marcus, *Rev Mod Phys*, 1993, 65, 599-610.

69. K. Tarafder, Y. Surendranath, J. H. Olshansky, A. P. Alivisatos and L. W. Wang, *J Am Chem Soc*, 2014, 136, 5121-5131.
70. T. Bak, J. Nowotny, M. Rekas and C. C. Sorrell, *J Phys Chem Solids*, 2003, 64, 1069-1087.
71. P. Odier, J. F. Baumard, D. Panis and A. M. Anthony, *J Solid State Chem*, 1975, 12, 324-328.